AIP Advances

Low temperature deposition of vanadium dioxide on III–V semiconductors and integration on mid-infrared quantum cascade lasers

Cite as: AIP Advances **13**, 015315 (2023); https://doi.org/10.1063/5.0111159
Submitted: 18 July 2022 • Accepted: 28 November 2022 • Published Online: 20 January 2023

Laurent Boulley, Thomas Maroutian, Paul Goulain, et al.

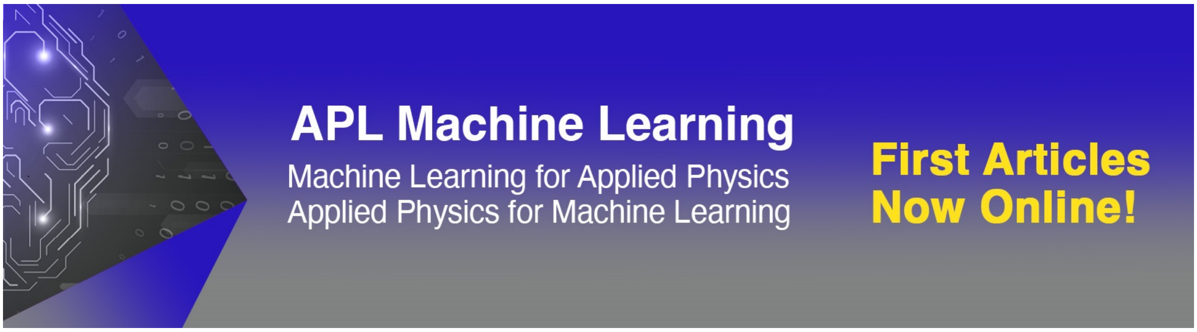

AIP Advances ARTICLE scitation.org/journal/adv

Low temperature deposition of vanadium dioxide on III–V semiconductors and integration on mid-infrared quantum cascade lasers

Cite as: AIP Advances 13, 015315 (2023); doi: 10.1063/5.0111159
Submitted: 18 July 2022 • Accepted: 28 November 2022 •
Published Online: 20 January 2023

Laurent Boulley,[1] **Thomas Maroutian,**[1] **Paul Goulain,**[1] **Andrey Babichev,**[2,3] **Anton Egorov,**[3] **Lianhe Li,**[4] **Edmund Linfield,**[4] **Raffaele Colombelli,**[1] **and Adel Bousseksou**[1 a)]

AFFILIATIONS

[1] Centre de Nanosciences et de Nanotechnologies (C2N), CNRS UMR 9001, Université Paris-Saclay, 91120 Palaiseau, France
[2] Ioffe Institute, 194021 Saint Petersburg, Russia
[3] ITMO University, 197101 Saint Petersburg, Russia
[4] School of Electronic and Electrical Engineering, University of Leeds, Leeds LS2 9JT, United Kingdom

[a)] **Author to whom correspondence should be addressed:** adel.bousseksou@c2n.upsaclay.fr

ABSTRACT

We demonstrate low temperature deposition conditions for vanadium dioxide (VO_2) phase change material by pulsed laser deposition, which are compatible with III–V semiconductors heterostructures typically used in optoelectronic applications. The characterizations of the VO_2 coated thin films grown on GaAs show a 50% change in optical reflectivity in the mid-infrared range and a variation of electric conductivity of two orders of magnitude between the insulating (low temperature) and the metallic (high temperature) states. The transition temperature is estimated around 68 °C (341 K). We also study the functionalization of mid-infrared quantum cascade lasers (QCLs) (operating at wavelengths $\lambda \sim 7$–$8\ \mu$m) with VO_2 layers, in view of engineering the laser emission properties with an integrated VO_2 layer. We demonstrate QCLs that integrate a VO_2 layer on the surface that interacts with the guided laser mode. A maximum operating temperature of 61 °C (334 K) has been measured.

The integration of phase change materials on III–V semiconductors devices represents an original and powerful solution to introduce new functionalities, thanks to the physical changes in these materials during the phase transition. It enables the realization of new monolithic, robust, compact, temperature tunable devices, be they active or passive, in the mid-infrared (mid-IR) wavelength range of 3–24 μm.

Vanadium dioxide (VO_2) is a phase change material that presents a metal–insulator transition (MIT) around 68 °C (Morin, 1959; Shao *et al.*, 2018), evolving from a monoclinic insulating phase below the MIT temperature to a rutile hexagonal metallic phase above (Baum *et al.*, 2007; Eyert, 2002; Rogers, 1993). VO_2 also presents the narrowest above room temperature (RT) phase transition among all the functional oxides available (Yang *et al.*, 2011), thus enabling the realization of simple devices without cooling or elevated heating temperature requirements.

VO_2 presents low optical losses in the mid-IR range (Dicken *et al.*, 2009) in its insulating phase due to a bandgap of 0.65 eV (Qazilbash *et al.*, 2007; Kats *et al.*, 2013). This bandgap reduces and closes with the temperature increase above 68 °C to obtain the metallic phase (Zylbersztejn and Mott, 1975). The insulating to metallic behavior changes the electric conductivity and, therefore, the permittivity, the refractive index, and the optical reflectivity (Choi *et al.*, 1996; Qazilbash *et al.*, 2009; Kats *et al.*, 2012; 2013). The generalized dielectric constant model describes the relationship among the electric conductivity $\sigma(\omega)$, the dielectric permittivity $\varepsilon_r(\omega)$, and the refractive index $n(\omega)$ (Ashcroft and Mermin, 1976),

$$\varepsilon_r(\omega) = n^2(\omega) = \varepsilon_\infty + i\frac{\sigma(\omega)}{\varepsilon_0\omega}, \tag{1}$$

where ω is the pulsation, ε_0 is the vacuum permittivity, and ε_∞ is the permittivity for infinite pulsation.

Pulsed laser deposition (PLD), radio frequency magnetron sputtering, and electron beam evaporation are the three main techniques employed for the deposition of VO_2 thin films (Marvel *et al.*, 2015). These growth techniques usually require lattice matched substrates such as c (0001) oriented sapphire substrates (Choi *et al.*, 1996; Bialas *et al.*, 1999; Wong *et al.*, 2013; Garry *et al.*, 2004) or silicon substrates (Tsai *et al.*, 2003; Roul *et al.*, 2021). VO_2 deposition processes are often done at high temperature (600–700 °C) and with a deposition pressure of around 10–30 mTorr (Choi *et al.*, 1996; Peng *et al.*, 2013; Wang *et al.*, 2016; Kim and Kwok, 1994; Garry *et al.*, 2004; Lee *et al.*, 2014; Prayakarao *et al.*, 2016; Gupta *et al.*, 2010).

VO_2 based perfect absorbers (Kats *et al.*, 2012), electronic switches (Crunteanu *et al.*, 2010; Dumas-Bouchiat *et al.*, 2007; Sanphuang *et al.*, 2015), and tunable metasurfaces (Kats *et al.*, 2013) have already been demonstrated on sapphire or bulky materials, in which structures are not affected by high temperature deposition conditions. Using those conditions for III–V semiconductors heterostructures would induce inter-diffusion in the alloys between quantum wells and barriers, essentially damaging the physical properties. Furthermore, the lattice mismatch between VO_2 in its rutile phase (lattice parameters a = b = 4.55 Å; c = 2.85 Å) (Eyert, 2002; Rogers, 1993; Bialas *et al.*, 1999; Wong *et al.*, 2013) and typical III–V semiconductors (a = b = c = 5.87 Å for InP) (Palik, 1998) does not fulfill the conditions for epitaxial growth of a monocrystalline film.

In this work, we develop and experimentally demonstrate new growth conditions for VO_2 thin films on GaAs and $In_{0.53}Ga_{0.47}As$ heterostructures by using PLD. The optimization of the deposition conditions enabled a much lower deposition temperature. The measured temperature on the heater thermocouple was 460 °C, resulting in a temperature of ~430 °C on the sample holder position. These optimized conditions lead to polycrystalline films that overcome the lattice mismatch problem. We demonstrate that the resulting surface roughness of ~20 nm root mean square (rms) does not hamper the device operation in the mid-IR range because it is much smaller than the optical wavelength (3–24 μm).

The VO_2 films were grown by using a PLD reactor (Peng *et al.*, 2013; Cheung and Horwitz, 1992) with a pulsed KrF excimer laser (λ = 248 nm) and a V_2O_5 ceramic target under controlled dioxygen flux. The target–substrate distance is 5 cm, and the deposition is homogeneous on a surface of ~1 cm^2. The initial VO_2 depositions were conducted on bulk GaAs and on $In_{0.53}Ga_{0.47}As/Al_{0.48}In_{0.52}As$ semiconductors heterostructures on the InP substrate. The samples were prepared to be the most vicinal to reach a roughness of 0.5 nm rms. They were first cleaned in acetone, isopropanol, then in an oxygen plasma, and de-oxidized in a diluted hydrochloric acid solution. They were then stuck on the PLD heating bar where the temperature was set to 460 °C.

At this temperature, in accordance with the V–O phase diagram (Kang, 2012), oxygen atomic fraction is located in a very narrow stability domain comprised between 0.645 and 0.670 in order to obtain the VO_2 phase (Kang, 2012; Bahlawane and Lenoble, 2014; Wriedt, 1989). Thus, the oxygen partial pressure (P_{O_2}) was limited to 1 mTorr in accordance with the Ellingham diagram (Lopez *et al.*, 2002).

To avoid an excessive deposition speed, the laser fluence and repetition frequency were set to 1.6 J·cm^{-2} and 5 Hz, respectively. The sample temperature, the laser fluence, and the repetition laser frequency are all decreased compared to what is often used in PLD references (Choi *et al.*, 1996; Peng *et al.*, 2013; Wang *et al.*, 2016; Kim and Kwok, 1994; Garry *et al.*, 2004; Lee *et al.*, 2014; Prayakarao *et al.*, 2016; Gupta *et al.*, 2010). We typically obtain VO_2 films of H_{VO_2} = 150 nm thickness with a total of 10^4 laser pulses. A post deposition sample annealing due to a very low inertial thermal cooling of the PLD heating bar, from 460 °C to RT, is performed to allow residual stress relaxation.

X-ray diffraction measurements (not shown) in the θ–2θ configuration gave information about the crystalline structure of the deposited films. The peaks obtained are large and of low amplitude, meaning that there is no epitaxial growth and that the films are polycrystalline. A roughness of less than 20 nm rms has been measured with atomic force microscopy (not shown).

Optical reflectivity characterizations of the samples have been carried out with an optical microscope coupled to a Fourier transform infrared (FTIR) spectrometer by using a mercury cadmium telluride cooled detector and globar mid-IR source in quasi-normal incidence. The reflectivity measurements have been performed below and above the VO_2 transition temperature by using a regulated heating and cooling platform. A schematic of the measurement principle is shown in the inset of Fig. 1(a).

Figure 1(a) shows the reflectivity measurements in the 1000–2500 cm^{-1} spectral range (λ = 4–10 μm) of a H_{VO_2} = 150 nm thick VO_2 film deposited on a GaAs substrate. The reflectivity spectra are divided by a reference spectrum obtained from a perfectly reflecting gold sample. The reflectivity R changes during the transition from R = 0.3 at 30 °C, where VO_2 is insulating, to R = 0.8 at 90 °C, where it is metallic. The film reflectivity is quasi flat at high temperature in the metallic state. It is also quasi flat at low temperature as there is no phonon absorption band in this measurement range (Barker *et al.*, 1966; Peng *et al.*, 2013). This significant change in optical reflectivity is due to the first order thermodynamic character of the VO_2 MIT (Choi *et al.*, 1996; Berglund and Guggenheim, 1969).

Noticeable is that the system is heterogeneous during the transition because the energy transfer is not instantaneous and each zone of the sample does not change in phase at the same time. On both sides of the temperature transition exists a metastable zone, which can lead to a delay in the transition and implies a hysteresis behavior (Choi *et al.*, 1996). The transition can be described as a percolation transition, nucleation, and growth of metallic (or rather insulating) grains in an insulating (or rather metallic) matrix occurring when temperature increases (or rather decreases) (Choi *et al.*, 1996; Qazilbash *et al.*, 2009; Qazilbash *et al.*, 2007; Qazilbash *et al.*, 2011). Figure 1(b) shows the hysteresis cycle for the reflectivity measurements for the same sample at a fixed wavelength of 8 μm for increasing and decreasing temperatures around the MIT temperature.

In addition, electrical characterizations were performed to measure the electric conductivity of the deposited VO_2 films on an insulating sapphire Al_2O_3 substrate by using the same optimized deposition conditions as presented above. Figure 2(a) presents a schematic view of the realized sample. Electrical contact pads adapted to transmission line measurements (TLM) were designed with optical lithography, evaporated (Ti/Au), and revealed by lift-off. Pads' length is W_1 = 100 μm and width is W_2 = 75 μm. They are

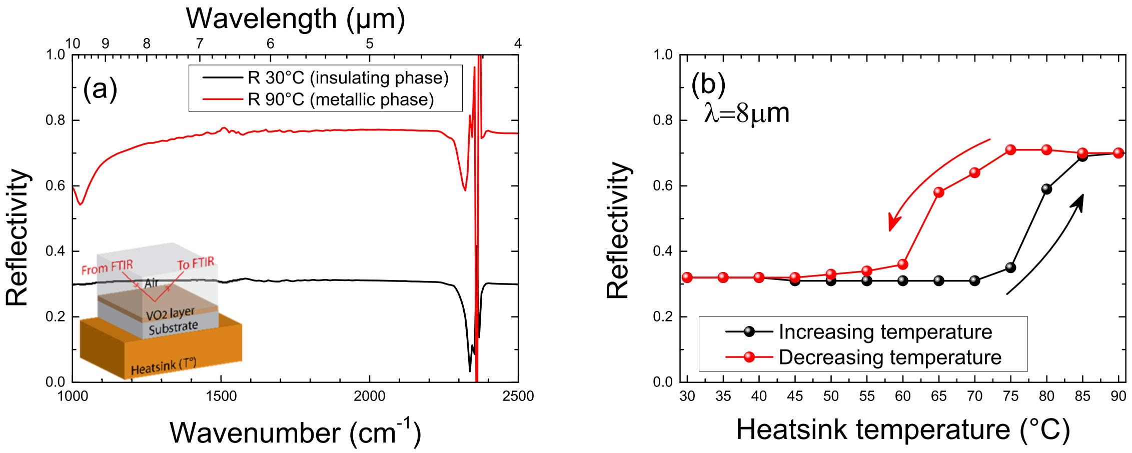

FIG. 1. (a) Measurement of the reflectivity of $H_{VO_2} = 150$ nm VO_2 layer deposited on GaAs substrate (PLD2971) below (30 °C) and above (90 °C) the phase transition temperature (68 °C). Inset: schematic of the sample for the reflectivity measurement. (b) Measurement of the reflectivity hysteresis cycle for increasing/decreasing temperatures between 30 and 90 °C at a fixed wavelength $\lambda = 8\ \mu$m.

separated by a distance L_{ij} (varying from 100 to 550 μm). The VO_2 film was laterally etched to avoid lateral leakage currents.

Measurements of the electric intensity-voltage $I(V)$ dependence between two pads give access to the total resistance R_T, which is defined as

$$R_T = \rho_{VO_2} \frac{L_{ij}}{W_1 H_{VO_2}} + 2R_C, \qquad (2)$$

where R_C is the pad contact resistance and ρ_{VO_2} is the electric resistivity of the VO_2 film. A linear regression provides a straight line, whose slope is equal to $\rho_{VO_2}/(W_1 H_{VO_2})$. Figure 2(b) plots the measured electric conductivity $\sigma_{VO_2} = 1/\rho_{VO_2}$ variation vs temperature of a $H_{VO_2} = 150$ nm thick VO_2 film. The measurements are reported for an increase and a decrease in temperature between 30 and 90 °C. It enables visualization of the transition phase and of the hysteresis occurring around 68 °C. σ_{VO_2} increases by more than two orders of magnitude from 0.4 to 80 S·cm^{-1} between 30 and 90 °C. We observe a hysteresis cycle between 63 and 77 °C as in the optical measurements.

VO_2 deposition on InGaAs/AlInAs heterostructures was finally addressed to create a VO_2 surface covered mid-IR quantum cascade laser (QCL). With the deposition of a 150 nm thickness VO_2 layer on the top surface of a QCL, the optical properties and the vertical confinement of the laser waveguide modes are modified according to the MIT. Thanks to the VO_2 refractive index variation, the optical confinement is dielectric below 68 °C and is surface plasmon like (Maier, 2007) above 68 °C. A maximum interaction between the waveguided optical laser mode and the top deposited VO_2 layer occurs when no low index spacer is introduced in between.

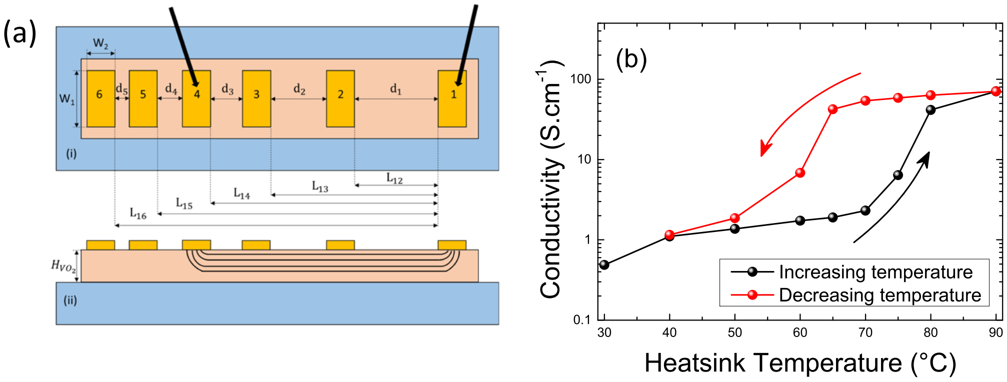

FIG. 2. (a) Schematic of the TLM samples. (i) Top view. Arrows represent the two metallic tips used in the measurement, here between pads 1 and 4. (ii) Side view. Current lines circulating in the VO_2 thin coating between the two contacted pads are represented (black curves). Sapphire substrate is in blue, VO_2 film in orange, and gold pads in yellow. (b) Measurement of the conductivity hysteresis cycle for increasing/decreasing temperatures between 30 and 90 °C. VO_2 shows a change in the conductivity of more than two orders of magnitude on either side of the transition (68 °C).

Nevertheless, this configuration induces high optical waveguide losses when VO_2 becomes metallic.

To implement a VO_2 top layer on QCL as schematized in the inset of Fig. 3(b), we optimized the QCL optical waveguide structure to maximize the optical confinement factor in the active region (Γ) while minimizing the waveguide propagation losses (α). Γ is defined as the ratio between the laser optical mode intensity concentrated in the active region and the total mode intensity.

We studied the effect of the insertion of a supplemental low index InP buffer layer ($n_{InP} = 3.1$ at 7.5 μm wavelength) between the active region ($n_{\text{Active Region}} = 3.4$ at 7.5 μm wavelength) and the top surface VO_2 layer in its dielectric and metallic phases. Figure 3(a) gives Γ and α as functions of the InP buffer thickness H_{InP_buff} using 2D transfer matrix waveguide numerical calculations. In the dielectric case, α is not affected by the InP buffer thickness and is about 3.5 cm^{-1}. A maximum Γ value of 0.8 is obtained for $H_{InP\_buff} = 0.75$ μm.

In the metallic case, Γ is maximum when there is no InP buffer layer ($H_{InP\_buff} = 0$ μm), α is maximum (35.8 cm^{-1}), and the mode intensity profile is concentrated at the metal/active region interface, typical of a quasi-plasmonic mode, thus maximizing the interaction between the top surface layer and the laser waveguided mode. A $H_{InP\_buff} = 0.75$ μm reduces the quasi-plasmonic losses of ~1/3 ($\alpha = 11$ cm^{-1}) and, thus, can guarantee good QCL operating features, especially at temperatures above the VO_2 MIT temperature. Conversely, the optical mode interacts less with the metallic top layer. Figure 3(b) plots the calculated mode energy density vertical profile for the dielectric and metallic cases. The metallic case exhibits a ~44% ratio between its maximum and its value at the metal/InP buffer interface, which constitutes a good interaction between the top surface layer and the laser waveguided mode.

The optimized QCL heterostructure with $H_{InP\_buff} = 0.75$ μm was grown in a molecular beam epitaxy reactor system. It contains 50 repeats of a four-well active region and injector with a total thickness of 2.635 μm. The targeted emission wavelength is $\lambda = 7.5$ μm. The QCL devices were processed as standard wet-etched laser ridges and are typically 22 μm wide and a few millimeters long (Bousseksou *et al.*, 2008). Additional steps were added to adapt to the optimized structure covered by a deposited VO_2 layer. A reactive ion etching fluorine plasma CF_4:O_2 was used to etch VO_2 and keep only an 8 μm wide strip on the top laser ridge surface. A 300 nm-thick Si_xN_y layer was thereafter deposited by plasma enhanced chemical vapor deposition to ensure lateral electrical insulation. For fabrication issues, the Si_xN_y layer deposited on top of the VO_2 layer was kept [see Fig. 3(b)]. Noteworthy is that the deposition of the Si_xN_y layer on the VO_2 layer during the laser process does not influence the laser properties because it is insulating and its refractive index is close to the VO_2 one (Dicken *et al.*, 2009). Figure 4(a) inset shows a false colorized top scanning electron microscopy (SEM) image of our processed VO_2 based QCL device.

The sample was mounted in a temperature regulated cryostat coupled to a FTIR spectrometer for optoelectrical characterizations. Figure 4(a) gives typical light-bias-current measurements as a function of the sample temperature. The electrical measurements were performed in a pulsed regime, typically 50 ns pulse width and 84 kHz repetition rate, in order to avoid thermal heating due to the electrical injection, excepted the measures at 300 and 334 K, which were done at a lower frequency of 55 kHz to better limit thermal heating. A threshold current of 2 kA·cm^{-2} at 78 K is measured. A maximum operating temperature of 334 K (61 °C) with a threshold current of 10.5 kA·cm^{-2} is obtained. The emitted spectrum [inset of Fig. 4(b)] shows typical Fabry–Perot modes centered at 7.8 μm wavelength. The maximum operating temperature is very close to the VO_2 MIT temperature (note that the temperature is measured at the bottom of the heat sink support, and a difference of a few degrees may occur with the top ridge surface). From one degree above 334 K, we observe an abrupt vanishing of laser emission, although the maximum injection current density is larger than 16 kA·cm^{-2} as shown in Fig. 4(a). One can expect that this sudden change is due to the phase change of the VO_2 top layer, which affects the waveguide optical losses.

To understand the behavior of our VO_2 based QCL devices [config. 1 in Fig. 4(b)], we processed two additional waveguide

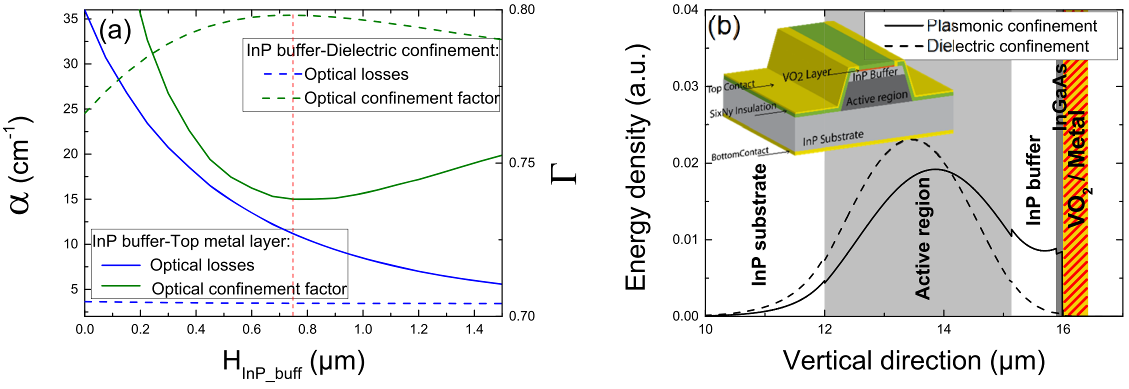

FIG. 3. (a) Calculations of the optical losses α (blue curves) and the optical confinement factor Γ (green curves) according to the inserted InP buffer thickness H_{InP_buff} for the dielectric confinement waveguide (dashes) and for the top Au metal layer surface plasmon waveguide (full lines). A maximum confinement of $\Gamma = 0.8$ is obtained in the dielectric confinement waveguide for a $H_{InP\_buff} = 0.75$ μm and corresponding optical losses are $\alpha = 3.45$ cm^{-1} (red vertical dashes). (b) Corresponding calculated mode energy density vertical profiles for $H_{InP\_buff} = 0.75$ μm and a dielectric confinement waveguide, simulating the VO_2 dielectric state (dashes) and a plasmonic waveguide with a gold top layer simulating a perfect VO_2 metallic state (full line). Inset: 3D schematic of the optimized VO_2 top surface QCL facet with InP buffer layer.

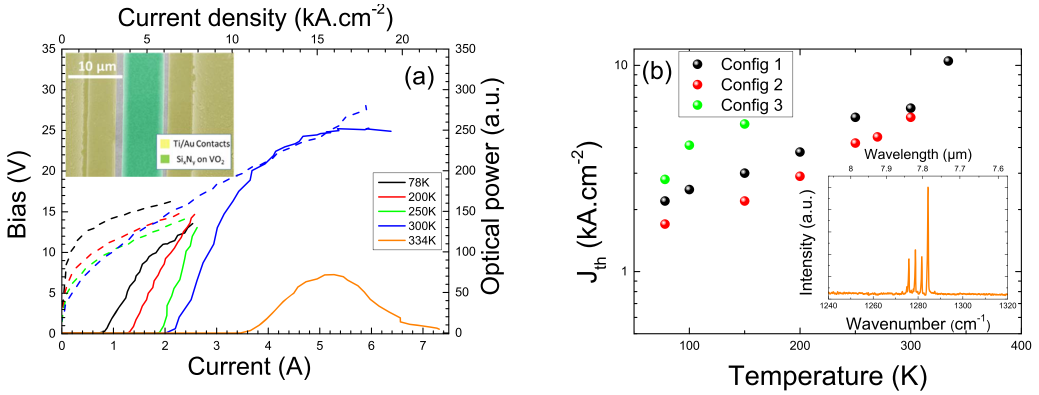

FIG. 4. (a) Current–voltage *I*(*V*) curves (dashes) and optical power–current curves (full lines) for the $H_{InP\_buff} = 0.75\ \mu m$ optimized VO$_2$ QCL. Inset: colorized SEM image of the fabricated structure. VO$_2$ is etched and forms a central strip on the top of the laser ridge with insulating Si$_x$N$_y$ layer added above (in green). Lateral Ti/Au contacts are taken on the top of the QCL (in yellow). (b) Threshold currents vs temperature. Black circles: VO$_2$ based QCL device (config. 1). Red circles: device where $H_{InP\_buff} = 0.75\ \mu m$ and the VO$_2$ top layer is replaced by a Ti/Au contact layer (config. 2). Green circles: device where $H_{InP\_buff} = 0\ \mu m$ and the VO$_2$ top layer is replaced by a Ti/Au contact layer (config. 3). Inset: emitted spectrum for the VO$_2$ based QCL at the maximum temperature of 334 K (61 °C).

configurations: one where $H_{InP\_buff} = 0.75\ \mu m$ and the VO$_2$ top layer is replaced by a Ti/Au contact layer [config. 2 in Fig. 4(b)], and the other where $H_{InP\_buff} = 0\ \mu m$ and the VO$_2$ top layer is replaced by a Ti/Au contact layer [config. 3 in Fig. 4(b)]. In Fig. 4(b), we plot the evolution of the measured current density thresholds as a function of the heat sink temperature for these three configurations. As can be expected, the InP buffer-less structure (config. 3) has the highest thresholds, mainly due to higher optical waveguide losses induced by the quasi-plasmonic character of the laser mode and the high interaction at the metal/active region interface. This is also coherent with waveguide loss calculations shown in Fig. 3(a). Unexpectedly, the VO$_2$ (in the dielectric phase) based optimized samples (config. 1) show slightly higher thresholds than the gold based optimized structures (config. 2). This can be explained by the inhomogeneous top surface lateral electrical injection.

To conclude, we develop in this study a new method for the deposition of VO$_2$ at low temperature in a way compatible with III–V semiconductors heterostructures. VO$_2$ layers show a change of more than 50% for the optical reflectivity and of more than two orders of magnitude for the electric conductivity between the dielectric state at low temperature and the metallic state at high temperature. We develop a new heterostructure laser waveguide that optimizes waveguide optical losses and the top layer/laser mode interaction, thanks to the addition of a top InP buffer. We demonstrate VO$_2$ based QCLs operating at 7.8 μm wavelength. The maximum operating temperature of 334 K has been achieved. It is limited by the phase change of the top VO$_2$ layer that switches in its metallic phase and induces sudden high optical waveguide losses. Considering further developments of this work, improvement of the VO$_2$ dielectric/metallic switching could be achieved by using higher performance QCL active regions (Wang *et al.*, 2021; Faist *et al.*, 2001). Furthermore, applying local electrical excitation to the VO$_2$ top layer could switch on its metallic phase without heating the whole QCL active region, considering thermal transfer during the MIT, which is minimized (Berglund and Guggenheim, 1969; Lee *et al.*, 2017), a property that can be taken advantage of in VO$_2$ based applications. Local electrical excitation can be as fast as the phase change transition timescale (Baum *et al.*, 2007), enabling high speed VO$_2$ based devices.

We acknowledge financial support from the French research agency ANR, grant ATLAS (Grant No. ANR-14-CE26-0004-01) and the Agence Française pour la Promotion de l'Enseignement Supérieur, l'Accueil et la Mobilité Internationale - Campus France (Project No. 38256QC). This work was partly supported by the French RENATECH network cleanroom facilities. We thank J.-M. Manceau, P. Lecoeur, and G. Agnus for the useful scientific exchange.

AUTHOR DECLARATIONS

Conflict of Interest

The authors have no conflicts to disclose.

Author Contributions

Laurent Boulley: Conceptualization (equal); Data curation (equal); Formal analysis (equal); Investigation (equal); Methodology (equal); Validation (equal); Visualization (equal); Writing – original draft (equal); Writing – review & editing (equal). **Thomas Maroutian**: Resources (equal); Validation (equal); Writing – review & editing (equal). **Paul Goulain**: Data curation (supporting); Investigation (supporting); Validation (supporting). **Andrey Babichev**: Investigation (supporting); Resources (supporting); Writing – review & editing (supporting). **Anton Egorov**: Resources (supporting). **Lianhe Li**: Resources (supporting). **Edmund Linfield**: Resources (supporting). **Raffaele Colombelli**: Conceptualization (equal); Formal analysis (equal); Funding acquisition (equal); Investigation (supporting); Methodology (supporting); Resources (equal); Supervision (supporting); Validation (equal); Visualization (equal); Writing – original draft (supporting); Writing – review & editing (supporting). **Adel Bousseksou**: Conceptualization (equal); Data curation (equal);

Formal analysis (equal); Funding acquisition (equal); Investigation (equal); Methodology (equal); Project administration (equal); Resources (equal); Supervision (equal); Validation (equal); Visualization (equal); Writing – original draft (equal); Writing – review & editing (equal).

DATA AVAILABILITY

The data that support the findings of this study are available within the article.

REFERENCES

Ashcroft, N. W. and Mermin, N. D., *Solid State Physics*, HRW international editions (Holt, Rinehart and Winston, 1976), p. 533.

Bahlawane, N. and Lenoble, D., "Vanadium oxide compounds: Structure, properties, and growth from the gas phase," Chem. Vap. Deposition **20**(7–9), 299–311 (2014).

Baum, P., Yang, D.-S., and Zewail, A. H., "4D visualization of transitional structures in phase transformations by electron diffraction," Science **318**(5851), 788–792 (2007).

Barker, A. S., Verleur, H. W., and Guggenheim, H. J., "Infrared optical properties of vanadium dioxide above and below the transition temperature," Phys. Rev. Lett. **17**(26), 1286–1289 (1966).

Berglund, C. N. and Guggenheim, H. J., "Electronic properties of VO_2 near the semiconductor-metal transition," Phys. Rev. **185**, 1022–1033 (1969).

Bialas, H., Dillenz, A., Downar, H. *et al.*, "Epitaxial relationships and electrical properties of vanadium oxide films on *r*-cut sapphire," Thin Solid Films **338**(1–2), 60–69 (1999).

Bousseksou, A., Moreau, V., Colombelli, R. *et al.*, "Surface-plasmon distributed-feedback mid-infrared quantum cascade lasers based on hybrid plasmon/air-guided modes," Electron. Lett. **44**(13), 807–808 (2008).

Cheung, J. and Horwitz, J., "Pulsed laser deposition history and laser-target interactions," MRS Bull. **17**(2), 30–36 (1992).

Choi, H. S., Ahn, J. S., Jung, J. H. *et al.*, "Mid-infrared properties of a VO_2 film near the metal-insulator transition," Phys. Rev. B **54**(7), 4621–4628 (1996).

Crunteanu, A., Givernaud, J., Leroy, J. *et al.*, "Voltage- and current-activated metal–insulator transition in VO_2-based electrical switches: A lifetime operation analysis," Sci. Technol. Adv. Mater. **11**(6), 065002 (2010).

Dicken, M. J., Aydin, K., Pryce, I. M. *et al.*, "Frequency tunable near-infrared metamaterials based on VO_2 phase transition," Opt. Express **17**(20), 18330 (2009).

Dumas-Bouchiat, F., Champeaux, C., Catherinot, A. *et al.*, "RF-microwave switches based on reversible semiconductor-metal transition of VO_2 thin films synthesized by pulsed-laser deposition," Appl. Phys. Lett. **91**(22), 223505 (2007).

Eyert, V., "The metal-insulator transitions of VO_2: A band theoretical approach," Ann. Phys. **11**(9), 650–704 (2002).

Faist, J., Beck, M., Aellen, T., and Gini, E., "Quantum-cascade lasers based on a bound-to-continuum transition," Appl. Phys. Lett. **78**(2), 147–149 (2001).

Garry, G., Durand, O., and Lordereau, A., "Structural, electrical and optical properties of pulsed laser deposited VO_2 thin films on R- and C-sapphire planes," Thin Solid Films **453–454**, 427–430 (2004).

Gupta, A., Narayan, J., and Dutta, T., "Near bulk semiconductor to metal transition in epitaxial VO_2 thin films," Appl. Phys. Lett. **97**(15), 151912 (2010).

Kang, Y.-B., "Critical evaluation and thermodynamic optimization of the VO–$VO_{2.5}$ system," J. Eur. Ceram. Soc. **32**(12), 3187–3198 (2012).

Kats, M. A., Blanchard, R., Genevet, P. *et al.*, "Thermal tuning of mid-infrared plasmonic antenna arrays using a phase change material," Opt. Lett. **38**(3), 368 (2013).

Kats, M. A., Blanchard, R., and Zhang, S., *et al.*, "Vanadium dioxide as a natural disordered metamaterial: Perfect thermal emission and large broadband negative differential thermal emittance," Phys. Rev. X **3**(4), 041004 (2013).

Kats, M. A., Sharma, D., Lin, J. *et al.*, "Ultra-thin perfect absorber employing a tunable phase change material," Appl. Phys. Lett. **101**(22), 221101 (2012).

Kim, D. H. and Kwok, H. S., "Pulsed laser deposition of VO_2 thin films," Appl. Phys. Lett. **65**, 3188–3190 (1994).

Lee, S., Hippalgaonkar, K., Yang, F. *et al.*, "Anomalously low electronic thermal conductivity in metallic vanadium dioxide," Science **355**(6323), 371–374 (2017).

Lee, S., Meyer, T. L., Park, S. *et al.*, "Growth control of the oxidation state in vanadium oxide thin films," Appl. Phys. Lett. **105**(22), 223515 (2014).

Lopez, R., Boatner, L. A., Haynes, T. E. *et al.*, "Synthesis and characterization of size-controlled vanadium dioxide nanocrystals in a fused silica matrix," J. Appl. Phys. **92**(7), 4031–4036 (2002).

Maier, S. A., *Plasmonics: Fundamentals and Applications* (Springer, 2007).

Marvel, R. E., Harl, R. R., Craciun, V. *et al.*, "Influence of deposition process and substrate on the phase transition of vanadium dioxide thin films," Acta Mater. **91**, 217–226 (2015).

Morin, F. J., "Oxides which show a metal-to-insulator transition at the Neel temperature," Phys. Rev. Lett. **3**, 34–36 (1959).

Palik, E. D., *Handbook of Optical Constants of Solids, Academic Press Handbook Series* (Elsevier Science, 1998).

Peng, W. W., Niu, G., Tétot, R. *et al.*, "Insulator-metal transition of VO_2 ultrathin films on silicon: Evidence for an electronic origin by infrared spectroscopy," J. Phys.: Condens. Matter **25**(44), 445402 (2013).

Prayakarao, S., Mendoza, B., Devine, A. *et al.*, "Tunable VO_2/Au hyperbolic metamaterial," Appl. Phys. Lett. **109**(6), 061105 (2016).

Qazilbash, M. M., Brehm, M., Andreev, G. O. , "Infrared spectroscopy and nano-imaging of the insulator-to-metal transition in vanadium dioxide," Phys. Rev. B **79**(7), 075107 (2009); arXiv:0904.0294.

Qazilbash, M. M., Brehm, M., Chae, B.-G. *et al.*, "Mott transition in VO_2 revealed by infrared spectroscopy and nano-imaging," Science **318**(5857), 1750–1753 (2007); arXiv:0801.1171.

Qazilbash, M. M., Tripathi, A., Schafgans, A. A. *et al.*, "Nanoscale imaging of the electronic and structural transitions in vanadium dioxide," Phys. Rev. B **83**(16), 165108 (2011); arXiv:1109.3347.

Rogers, K. D., "An X-ray diffraction study of semiconductor and metallic vanadium dioxide," Powder Diffr. **8**(4), 240–244 (1993).

Roul, B., Singh, D. K., Pant, R. *et al.*, "Electrical transport modulation of VO_2/Si(111) heterojunction by engineering interfacial barrier height," J. Appl. Phys. **129**(24), 244502 (2021).

Sanphuang, V., Ghalichechian, N., Nahar, N. K. *et al.*, "Equivalent circuit for VO_2 phase change material film in reconfigurable frequency selective surfaces," Appl. Phys. Lett. **107**(25), 253106 (2015).

Shao, Z., Cao, X., Luo, H., and Jin, P., "Recent progress in the phase-transition mechanism and modulation of vanadium dioxide materials," NPG Asia Mater. **10**(7), 581–605 (2018).

Tsai, K.-Y., Chin, T.-S., and Shieh, H.-P. D., "Properties of VO_2 films sputter-deposited from V_2O_5 target," Jpn. J. Appl. Phys. **42**(7A), 4480–4483 (2003).

Wang, S., Liu, M., Kong, L. *et al.*, "Recent progress in VO_2 smart coatings: Strategies to improve the thermochromic properties," Prog. Mater. Sci. **81**, 1–54 (2016).

Wang, F., Slivken, S., and Razeghi, M., "High-brightness LWIR quantum cascade lasers," Opt. Lett. **46**, 5193–5196 (2021).

Wong, F. J., Zhou, Y., and Ramanathan, S., "Epitaxial variants of VO_2 thin films on complex oxide single crystal substrates with 3*m* surface symmetry," J. Cryst. Growth **364**, 74–80 (2013).

Wriedt, H. A., "The O-V (Oxygen-Vanadium) system," Bull. Alloy Phase Diagrams **10**(3), 271–277 (1989).

Yang, Z., Ko, C., and Ramanathan, S., "Oxide electronics utilizing ultrafast metal-insulator transitions," Annu. Rev. Mater. Res. **41**(1), 337–367 (2011).

Zylbersztejn, A. and Mott, N. F., "Metal-insulator transition in vanadium dioxide," Phys. Rev. B **11**, 4383–4395 (1975).